SCIENCE CHINA
Physics, Mechanics & Astronomy

• Article •

April 2026 Vol. 69 No. 4: 244211
https://doi.org/10.1007/s11433-025-2886-3

Non-reciprocal coupling induced chaotic states in nonlinear optical model

Penghong Yu[1†], Juan Chen[1,2†], Luojia Wang[1*], Yanyan He[1], Xiaoxiong Wu[1], Zhaohui Dong[1], Xianfeng Chen[1,3,4], and Luqi Yuan[1*]

[1] *State Key Laboratory of Advanced Optical Communication Systems and Networks, School of Physics and Astronomy, Shanghai Jiao Tong University, Shanghai 200240, China*
[2] *College of Physics and Communication Electronics, Jiangxi Normal University, Nanchang 330022, China*
[3] *Shanghai Research Center for Quantum Sciences, Shanghai 201315, China*
[4] *Collaborative Innovation Center of Light Manipulations and Applications, Shandong Normal University, Jinan 250358, China*

Received September 19, 2025; accepted January 4, 2026; published online February 5, 2026

We study an optical model including both non-reciprocal couplings and third-order nonlinearity. We find that such a model can generate chaotic states, with various characteristics such as intermittent chaos and asymmetric chaotic patterns. Moreover, after considering our model in an experimentally-feasible platform of coherent Raman scattering, the nonlinear coefficient becomes frequency-dependent, which can lead to unique consequences, including asymmetric localization of covariant Lyapunov vectors and the transition between low-dimensional chaos and spatiotemporal chaos. The generated chaotic frequency sidebands are featured by a broad frequency spectrum and notable asymmetry, offering significant opportunity for advancing quantum chaos theory and finding potential applications in light detection and ranging as well as Raman spectroscopy.

non-reciprocal coupling, chaos, coherent Raman scattering

Citation: P. Yu, J. Chen, L. Wang, Y. He, X. Wu, Z. Dong, X. Chen, and L. Yuan, Non-reciprocal coupling induced chaotic states in nonlinear optical model, Sci. China-Phys. Mech. Astron. **69**, 244211 (2026), https://doi.org/10.1007/s11433-025-2886-3

1 Introduction

Chaos, the phenomenon ubiquitous to nonlinear physics, observed by Poincare in 1905 and later explored by Lorenz equations [1], has been broadly observed in many-body problems [2-6], fluid dynamics [7-10], and optical effects [11-14]. The fascinating scientific aspect of studying chaos is due to its counterintuition that deterministic equations can be unpredictable [15]. In other words, a small deviation in initial conditions can be exponentially increasing, so the prediction of the precise dynamics of chaos at long time is difficult [15]. Great attentions have been applied in understanding the transition from ordered states to chaotic states [16, 17] and identifying underlying patterns within apparent randomness [18]. In optics, the analogy between the Maxwell-Bloch equations for light and the Lorenz equations has been noted for a long time [1, 11], and the corresponding optical chaos has then been extensively explored [19-23]. In particular, the nonlinear Schrödinger equation (NLSE) for the field $q(x,t)$:

$$iq_t + dq_{xx} + Q|q|^2 q = 0, \tag{1}$$

where the dispersion parameter d and the nonlinear parameter Q are constants, underpins key chaotic phenomena found in optics, including rogue waves [24], chaotic localized state [25], and chaotic microcombs [26, 27].

*Corresponding authors (Luojia Wang, email: ljwang@sjtu.edu.cn; Luqi Yuan, email: yuanluqi@sjtu.edu.cn)

†Equally contributed to this work

As the NLSE is a conservative equation, to generate chaotic states, one needs to add necessary perturbations into it [28]. For instance, the Lugiato-Lefever equation (LLE) [29], a damped and driven version of the NLSE, a damped and driven version of the NLSE but is open and exchanges energy with environment, has been extensively studied in the context of optical chaos, where perturbation is provided by the driving field and loss [30-34]. The intrinsic unpredictability and extreme sensitivity to perturbations in chaotic states may provide important applications in radar for high-resolution ranging [35, 36], secure communications [37-39], random number generation [40-44], and optical computing [45, 46]. However, while the resulting chaotic phenomena may appear asymmetric due to perturbations, the underlying mathematical framework of NLSE-based systems for chaos generation fundamentally preserves macroscopic inversion symmetry. This inherent symmetry imposes a limitation on the diversity of solutions [47].

This work tackles the problem of an NLSE-based system with the inversion symmetry breaking and shows the occurrence of chaotic states without additional perturbations. The non-reciprocal coupling, which has recently brought numerous important phenomena in optical systems [48-51], is used to break the inversion symmetry of the model. The non-reciprocal coupling also transforms the conservative NLSE into a non-Hermitian equation, which exchanges energy with the environment, such that the transition from periodic dynamics into a chaotic state is expected. We further confirm the chaos in the field evolution by the calculated positive maximal Lyapunov exponents (LEs). Moreover, by increasing the nonlinear strength, the field in the system experiences the transition from the periodic behavior to chaotic dynamics, through the intermittency route [15]. The chaotic nature of the irregular bursts is verified by the calculated positive local LEs [52]. Our model may be immediately feasible in experiments of coherent Raman scattering (CRS) processes [53-56]. The additional frequency-dependent nonlinear term in CRS can further lead to asymmetric localization of the covariant Lyapunov vectors of the positive LEs, and transit the system from low-dimensional chaos [57] to spatiotemporal chaos, where the frequency comb lines are orthogonal [27]. With all of the results, we demonstrate a novel way for generating chaotic states based on NLSE, which could be offered as a new candidate in the aforementioned and future applications and enrich the study of chaos theory.

2 Model and results

We begin by considering the periodic condition of x ($x = x + 2\pi/\Omega$) in eq. (1), which is a typical model in an optical ring platform [58], and Fourier-transforming eq. (1) from x to n. Here q is discretized into discrete components $q_n = \int_{-\pi}^{\pi} q(x,t)\exp[-i(n-n_c)x]\,\mathrm{d}x/2\pi$ with an oscillating frequency $\omega_n = n\Omega$. The integer n refers to a central index n_c and frequency spacing Ω between two nearby components. By taking dimensionless parameters: $E_n \equiv \sqrt{2\pi}q_n/\sqrt{\int_{-\pi}^{\pi}|q(x,t=0)|^2\mathrm{d}x}$, $\tau \equiv \Omega t$, $d_2 \equiv -d/\Omega$, and $g \equiv Q\int_{-\pi}^{\pi}|q(x,t=0)|^2\mathrm{d}x/2\pi\Omega$, we re-write NLSE in the frequency domain:

$$-i\frac{\partial E_n}{\partial \tau} = d_2(n-n_c)^2E_n + J_n(E_{n+1}+E_{n-1}) + g\sum_{m,p}E_m^*E_pE_{m+n-p}, \tag{2}$$

where d_2 is positive (negative) for normal (anomalous) dispersion. J_n is the coupling strength between nearby components. When $J_n = 0$, eq. (2) is identical to eq. (1) after the Fourier transformation. Nevertheless, the inclusion of the term with J_n brings the energy hopping between nearby components of E_n. We can further assume $J_n \propto n$ here to introduce the non-reciprocal couplings, where the energy hopping along the path from the n-th component to the $(n+1)$-th component is different from that of the reverse path, as shown in Figure 1(a), breaking the inversion symmetry in the NLSE. The last term in eq. (2) is referred to as four-wave mixing (FWM), as shown in Figure 1(b). In the following, we analyze the effect of the term with J_n and then discuss the potential realization of eq. (2) in a realistic experimental platform.

Here we first show that eq. (2) can support the transition from periodic evolution to chaotic dynamics. In our numerical simulations, eq. (2) is solved with 30 field components. The parameters are set to $d_2 = -1$, $n_c = 30$, $J_n = 2n$, with the initial condition $E_n(\tau = 0) = \delta_{n10}$. Figure 2(a)-(e) shows the evolution for field components $|E_n|^2$ under different nonlinear strengths $g = 0, 1, 2, 5, 10$, respectively. When there is no nonlinearity in the model ($g = 0$), the system exhibits periodic dynamics due to the dispersion-induced artificial boundaries in the frequency domain [59] (Figure 2(a)). However, once the nonlinearity is introduced, as shown in Figure 2(b)-(e), it significantly affects the evolution, leading the system to enter the chaotic regime (Figure 2(e)), after a transient phase

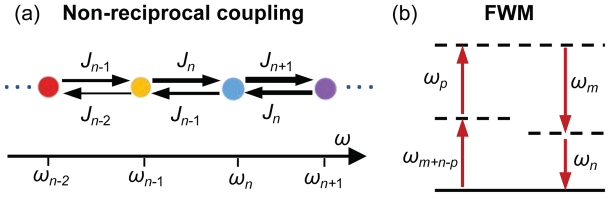

Figure 1 (Color online) (a) Illustration of non-reciprocal coupling between nearby frequency components with $J_n \propto n$. (b) Energy level diagram depicting FWM.

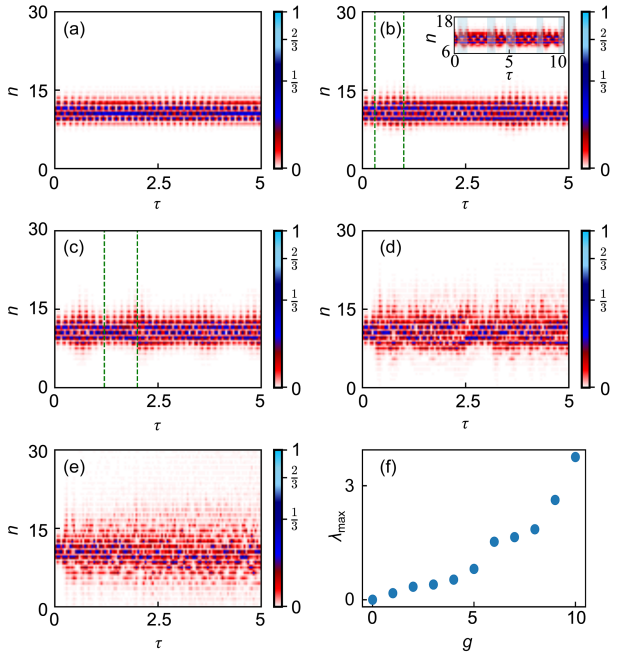

Figure 2 (Color online) Temporal evolution of the field component $|E_n|^2$ at different nonlinear strengths: (a) $g = 0$, (b) $g = 1$, (c) $g = 2$, (d) $g = 5$, and (e) $g = 10$. The region between the green dashed lines in (b) and (c) marks the formation of chaotic bursts. The inset shows the field evolution with $\tau \in [0,10]$. The chaotic bursts are indicated by the lightbule background. (f) Maximal LEs as a function of g.

[15, 52]. One can note that for larger g, the transient phase fades out quicker, with more components getting faster excited. Here we demonstrate that chaotic states can emerge in a nonlinear NLSE with artificially added non-reciprocal couplings, a behavior strictly prohibited in systems governed solely by eq. (1), which is conservative and integrable. This mechanism of chaos generation distinctly differs from conventional damped-and-driven schemes [47], and the distribution of field components is asymmetric due to the inversion symmetry breaking of the model.

To verify the occurrence of chaos in Figure 2(a)-(e) and quantify the chaos under different parameters, we calculate the maximal LE, defined as [15]:

$$\lambda_{\max} = \lim_{\tau\to\infty} \lim_{|\delta \boldsymbol{E}|\to 0} \frac{1}{\tau} \ln \frac{|\delta \boldsymbol{E}(\tau)|}{|\delta \boldsymbol{E}|}, \tag{3}$$

where $\delta \boldsymbol{E}$ is an infinitesimal initial displacement from $\boldsymbol{E}(0)$, and $\delta \boldsymbol{E}(\tau)$ is its evolved displacement at time τ. The maximal LE serves as a quantitative indicator of chaotic dynamics, with positive values ($\lambda_{\max} > 0$) signifying exponential divergence of nearby trajectories. The growth rate of this divergence scales with $\lambda_{\max}$. As shown in Figure 2(f), the monotonic increase of $\lambda_{\max}$ with the increasing g is consistent with the tendency of chaos observed in Figure 2(a)-(e). Moreover, the positive maximal LEs verify that our model reaches the chaotic regime.

We now identify the specific pathway from ordered to chaotic dynamics in our system. At weak nonlinearity ($g = 1, 2$), distinct bursts in Figure 2(b) and (c) intermittently disrupt the otherwise periodic evolution (Figure 2(a)), while stronger nonlinearity ($g = 10$) shows no such bursts, indicating a fully developed chaotic state (Figure 2(e)). To quantitatively characterize this pathway, we calculate the local LEs, defined as: $\lambda_{\text{local}} = \lim_{\tau\to 0} \lim_{|\delta \boldsymbol{E}|\to 0} \frac{1}{\tau} \ln(|\delta \boldsymbol{E}(\tau)|/|\delta \boldsymbol{E}|)$, and plot results in Figure 3. Our numerical results reveal a clear correlation: positive local LEs correspond precisely to the formation of the observed chaotic bursts, while the negative values indicate relaxation from bursts back to periodic evolution, as illustrated in Figure 3(b) and (c). Moreover, the inset of Figure 2(b) shows an alternating pattern between chaotic bursts and periodic motion, where the chaotic bursts are indicated by the lightbule regions, and they correspond to the peaks of local LEs in the inset of Figure 3(b). As the nonlinear strength g increases to 5, these bursts become more frequent until the system reaches full chaos, evidenced by predominantly positive local LEs (Figure 3(d)). This progression—from periodic behavior to fully developed chaos through intermittent bursts—indicates the intermittency route to chaos in our model.

Now, we give a realistic experimental platform that can support the construction of an NLSE with non-reciprocal couplings. We consider a CRS process [53-56], where a pair of pump pulses with the frequency difference Ω two-photon near-resonantly excite the molecular coherence in a Raman-active medium, and then a probe pulse is injected to interact with the coherence. During the propagation of the probe, equally spaced Raman sidebands across the spectrum can be

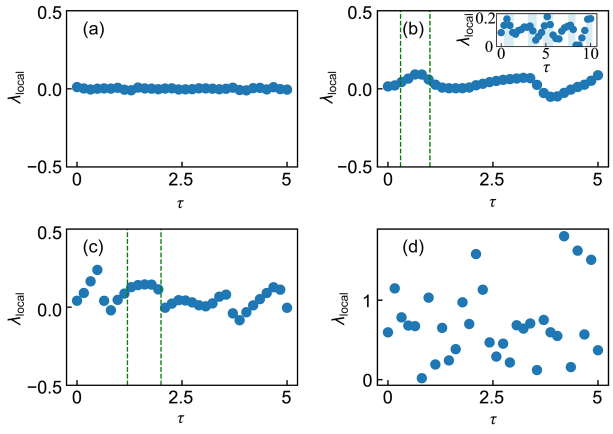

Figure 3 (Color online) Local LEs for (a) $g = 0$, (b) $g = 1$, (c) $g = 2$, and (d) $g = 10$. The green dashed lines mark the time intervals where the local LEs become positive, indicating the bursts observed in Figure 2(b) and (c) are chaotic. The inset of Figure 2(b) shows an alternating pattern between chaotic bursts and periodic motion, where the chaotic bursts are indicated by the lightbule regions, and they correspond to the peaks of local LEs in the inset of Figure 3(b).

generated. The wave equations for the decomposed Raman sidebands in the probe can be written as [55]:

$$-i\frac{\partial E_n}{\partial \tau} = d_2(n-n_c)^2 E_n + J_n(E_{n-1}+E_{n+1}) + g_n \sum_{m,p} E_m^* E_p E_{m+n-p}, \tag{4}$$

where $\tau \equiv z/z_c$ is still dimensionless, where z_c represents a characteristic distance. E_n is the electric field of the n-th sideband at frequency $\omega_n \equiv n\Omega$ for the simplicity.

Under typical experimental conditions in CRS, the group velocity dispersion can naturally make significant influence if we consider the solid Raman-active medium [56], which gives the term with d_2 in eq. (4). For the coherent Raman process, the hopping from the $(n+1)$-th sideband to the n-th sideband is determined by: $J_n = \omega_n l_0 |\varrho_{ab}| z_c = n\Omega l_0 |\varrho_{ab}| z_c \equiv nJ_1$, and the reverse hopping is $J_{n+1} = \omega_{n+1} l_0 |\varrho_{ab}| z_c \equiv (n+1)J_1$ [55], where ϱ_{ab} is the molecular coherence and l_0 is the transition coefficient of the two-photon molecular transition for all frequency components under the far-detuning approximation [53]. The last term in eq. (4) accounts for the FWM process of the probe sidebands, where $g_n = \omega_n n_{\rm NL} I_{\rm in} z_c/(2\pi A_{\rm eff} c) = n\Omega n_{\rm NL} I_{\rm in} z_c/(2\pi A_{\rm eff} c) \equiv n g_1$ [60]. Here, $n_{\rm NL}$ is the nonlinear refractive index across the spectrum of interest, I_{in} is the input power, $A_{\rm eff}$ is the effective pulse area, and c is the speed of light in vacuum. We clarify here that for the Raman sideband generations with visible or ultraviolet pulses, the frequency spacing Ω is typically on the order of 10-100 THz [61-63], which is non-negligible for any frequency-dependent parameters such as J_n and g_n.

Eq. (4) is similar to eq. (2) in the manner of its nonreciprocal NLSE. The difference is that g_n in the last term is n-dependent in eq. (4). We find that the chaotic state governed by eq. (4) also exhibits the intermittency route to chaos under the same initial conditions, as observed from eq. (2). Nevertheless, the difference between the two equations on the n-dependent nonlinearity g_n in eq. (4) brings two additional important features: the asymmetric localization of covariant Lyapunov vectors (CLVs) [64] and the generation of spatiotemporal chaos [27].

To characterize the CLV feature, we numerically compute the localization properties. $\delta\mathscr{E}(\tau) \equiv (\delta\mathscr{E}_1, ..., \delta\mathscr{E}_n, ..., \delta\mathscr{E}_N)^T \in \mathbb{R}^{2N}$, representing a small perturbation around $E(\tau)$, where $\delta\mathscr{E}_n$ labels the complex perturbation amplitude of the n-th sideband, with normalization $|\delta\mathscr{E}(\tau)| = 1$ maintained. Here, $\delta\mathscr{E}(\tau)$ corresponds to the maximal LE and indicates the local direction along which the perturbation vector grows at the highest exponential rate [65]. To quantitatively study CLVs, we calculate the group localization index ρ_n, defined as [65]:

$$\rho_n = N\frac{|{\rm Re}(\delta\mathscr{E}_n)|^2 + |{\rm Im}(\delta\mathscr{E}_n)|^2}{\sum_n |{\rm Re}(\delta\mathscr{E}_n)|^2 + |{\rm Im}(\delta\mathscr{E}_n)|^2}. \tag{5}$$

A large value of ρ_n indicates stronger CLV localization on the nth sideband, i.e., a perturbation of the field component on this sideband can grow faster, implying a higher perturbation sensitivity. Conversely, a small value of ρ_n implies weaker localization, and hence lower perturbation sensitivity. In Figure 4, we plot ρ_n using results simulated from eqs. (2) and (4) respectively, and the normalized averaged intensities $I_{\rm ave}(n) \equiv \lim_{\tau_0\to\infty} \int_0^{\tau_0} |E_n|^2 {\rm d}\tau/\tau_0$. One can see that ρ_n in two cases is different in higher sidebands, and in particular, in Figure 4(b), ρ_n scales differently from $I_{\rm ave}$ for $n > 5$. This mismatch reveals that the CLV localization is not solely governed by sideband intensity but indicates an intrinsic asymmetry induced higher-order sideband localization. This effect arises from the linear dependence of nonlinearity $g_n = ng_1$, which amplifies the sensitivity of perturbations in higher-frequency sidebands. Such behavior is reminiscent of chimera states [65], where CLVs are more localized for certain oscillators despite global coupling. Therefore, the asymmetric CLV localization implies chimeralike dynamics across globally coupled sidebands, with different perturbation sensitivity.

To see the feature of spatiotemporal chaos, we need to introduce cross correlation function [25]:

$$c(n_1,n_2) = \lim_{\tau_0\to\infty} \frac{\int_0^{\tau_0} E_{n_1}(\tau)E_{n_2}(\tau){\rm d}\tau}{\sqrt{\int_0^{\tau_0} |E_{n_1}(\tau)|^2{\rm d}\tau \int_0^{\tau_0} |E_{n_2}(\tau)|^2{\rm d}\tau}} \tag{6}$$

to quantitatively characterize the correlation between the sidebands (n_1, n_2), $n_1, n_2 \in \mathbb{N}^*$. In Figure 5(a) and (b), we perform simulations on eq. (4) with $J_n = 10g_n$ to find $E_n(\tau)$ and then plot the correlation matrix $|c(n_1,n_2)|$. One can see that a considerable degree of correlation remains between neighboring sidebands due to significant mutual dependence on adjacent sidebands from the strong non-reciprocal coupling J_n. This corresponds to low-dimensional chaos [57]. In contrast, when we apply simulations with $J_n = g_n$, and plot results in Figure 5(c) and (d), one sees that the sidebands exhibit negligible correlation with others, indicating the signature of spatiotemporal chaos [27]. Furthermore, the large frequency spacing inherent to the CRS process ensures that

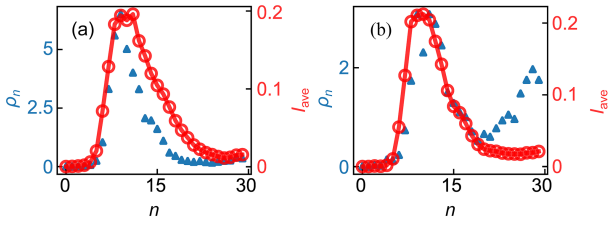

Figure 4 (Color online) The averaged intensities for each sideband along the evolution (red), group localization index ρ_n (blue) corresponds to the maximal LEs for (a) simulation results of eq. (2), (b) simulation results of eq. (4) with $g_n = n$.

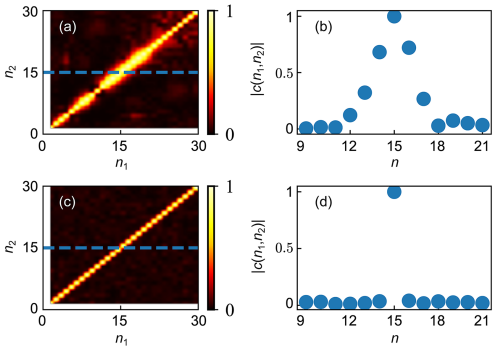

Figure 5 (Color online) Correlation in the frequency domain. Correlation between sidebands for (a) $J_n = 10g_n$ and (c) $J_n = g_n$; (b) and (d) show cross-sections along the dashed lines in (a) and (c), respectively.

these mutually uncorrelated sidebands can be individually addressed. Such a property in spatiotemporal chaos can be possibly beneficial for light detection and ranging (LiDAR) systems [26, 27], as it enables simultaneous ranging without self-interference, and hence enhances the potential for parallel detection.

3 Discussions and conclusion

The dimensionless framework adopted in eq. (4) corresponds to an experimentally attainable regime. A plausible implementation could consist of the following: a commercially available pulsed laser system delivering peak power $I_{\mathrm{m}} \sim 10^6$ W focused to an effective mode area $A_{\mathrm{eff}} \sim 10^{-3}$ mm^2; a nonlinear medium such as GaP, silicon, or GaN [63, 66, 67] with a nonlinear refractive index $n_{\mathrm{NL}} \sim 10^{-11}$ mm^2/W. The frequency detuning Ω can be taken as ~ 30 THz, which is comparable to the Raman shifts of Raman-active materials [68]. Then one can use a probe field with its wavelength near 1 μm, consistent with the initial condition 10 Ω used in simulations and two pumps with wavelengths around 300 nm. The characteristic length is chosen as $z_{\mathrm{c}} \sim 1$ cm, leading to a physical Raman sample length of approximately 5 cm. Other realistic parameters include a group velocity dispersion (GVD) $\sim -10^{-24}$ s^2/m [63], a molecular density $N \sim 10^{28}$ /m^3 [69], a pre-established coherence $|\varrho_{ab}| \sim 0.5$ [54], and a dipole moment $d_0 \sim 5 \times 10^{-8}$ [55].

When we derive eq. (4), we take several reasonable approximations. The first one is the slowly varying envelope approximation for the spatial dependence, that is, we assume that the variation of E in time and space occurs only over distances much larger than an optical wavelength. We also assume that the probe pulse interacts with the molecular coherence pre-prepared by the pump pulses, neglecting any change in coherence during the probe pulse. This simplification is valid if the probe pulse is sufficiently short, such that the molecular state remains largely unchanged. The nonlinear strength for the FWM of Raman sidebands is drastically simplified, where we neglect the frequency dependence of the effective pulse area and nonlinear refractive index. In simulations of eq. (4), we set $d_2 = -1$ for $n < 30$ and $d_2 = 4$ for other components. This approximation is made to ensure the anomalous dispersion in the frequency regime of interest. Our model may also be potentially realized in an optical ring resonator including the Kerr nonlinearity, where the non-reciprocal coupling between frequency components can be achieved by resonantly modulating the ring with both amplitude and phase modulators [70].

The chaotic state generation from eq. (4) can be generalized to other fiber or waveguide-based optical platforms [71-73]. The universal requirements for implementing eq. (4) are anomalous dispersion, non-reciprocal coupling, and frequency-dependent nonlinear strength. Anomalous dispersion is readily available in standard optical fibers within specific wavelength ranges [74], and can be obtained through waveguide geometry engineering [63]. Non-reciprocal coupling has been demonstrated in systems such as synthetic photonic lattices with gauge fields [70, 75]. Frequency-dependent nonlinear strength can be achieved through engineered modal confinement. For instance, in waveguides, the effective modal area can vary significantly with frequency [76], enabling substantial g_n variation even for small frequency separations.

In summary, we study optical chaos generated in an NLSE with inversion symmetry breaking that is induced by non-reciprocal coupling. Moreover, our work establishes a link between the long-studied field of chaos and the emerging concept of non-reciprocal coupling, or more broadly, non-Hermitian physics. The route to chaos is identified as the intermittency route. Moreover, we show that both chimeralike chaotic states and spatiotemporal chaos can emerge in our model, which can be possibly realized in the CRS process. Unlike previous works focusing on chaos in damped and driven NLSE [26-31], our approach introduces the distinctly asymmetric pattern, and also the transition between low-dimensional chaos and spatiotemporal chaos in the chaotic light generation, which holds promise for a variety of applications, including secure communications [37-39], optical computing [45, 46], random number generation [40-43, 77], and LiDAR [26, 27].

This work was supported by the National Key R&D Program of China (Grant No. 2023YFA1407200) and the National Natural Science Foundation of China (Grant Nos. 12122407, 12192252, and 12204304).

Conflict of interest The authors declare that they have no conflict of interest.

1 E. N. Lorenz, J. Atmos. Sci. **20**, 130 (1963).

2 J. Barrow-Green, Poincaré and the Three Body Problem. Providence: American Mathematical Soc. (1997).
3 P. Kos, M. Ljubotina, and T. Prosen, Phys. Rev. X **8**, 021062 (2018).
4 B. Kobrin, Z. Yang, G. D. Kahanamoku-Meyer, C. T. Olund, J. E. Moore, D. Stanford, and N. Y. Yao, Phys. Rev. Lett. **126**, 030602 (2021).
5 A. Frisch, M. Mark, K. Aikawa, F. Ferlaino, J. L. Bohn, C. Makrides, A. Petrov, and S. Kotochigova, Nature **507**, 475 (2014).
6 B. C. Yang, J. Pérez-Ríos, and F. Robicheaux, Phys. Rev. Lett. **118**, 154101 (2017).
7 W. D. McComb, The Physics of Fluid Turbulence. Oxford: Oxford University Press (1990).
8 J. M. Ottino, F. J. Muzzio, M. Tjahjadi, J. G. Franjione, S. C. Jana, and H. A. Kusch, Science **257**, 754 (1992).
9 K. R. Sreenivasan, Rev. Mod. Phys. **71**, S383 (1999).
10 A. Khodakaram-Tafti, H. Emdad, and M. Mahzoon, Chaos Solitons Fractals **179**, 114383 (2024).
11 H. Haken, Phys. Lett. A **53**, 77 (1975).
12 R. G. Harrison, and D. J. Biswas, Nature **321**, 394 (1986).
13 M. Sciamanna, and K. A. Shore, Nat. Photon. **9**, 151 (2015).
14 L. Fan, X. Yan, H. Wang, and L. V. Wang, Sci. Adv. **7**, eabc8448 (2021).
15 S. H. Strogatz, Nonlinear Dynamics and Chaos: With Applications to Physics, Biology, Chemistry, and Engineering. Boca Raton: CRC press (2018).
16 S. W. Haugland, A. Tosolini, and K. Krischer, Nat. Commun. **12**, 5634 (2021).
17 H. Kang, A. Zhou, Y. Zhang, X. Wu, B. Yuan, J. Peng, C. Finot, S. Boscolo, and H. Zeng, Phys. Rev. Lett. **133**, 263801 (2024).
18 J. P. Crutchfield, Nat. Phys. **8**, 17 (2012).
19 T. Yamada, and R. Graham, Phys. Rev. Lett. **45**, 1322 (1980).
20 K. Otsuka, and H. Kawaguchi, Phys. Rev. A **29**, 2953 (1984).
21 T. B. Simpson, J. M. Liu, A. Gavrielides, V. Kovanis, and P. M. Alsing, Appl. Phys. Lett. **64**, 3539 (1994).
22 H. Kawaguchi, Appl. Phys. Lett. **45**, 1264 (1984).
23 M. San Miguel, Q. Feng, and J. V. Moloney, Phys. Rev. A **52**, 1728 (1995).
24 D. R. Solli, C. Ropers, P. Koonath, and B. Jalali, Nature **450**, 1054 (2007).
25 L. Zhong, Q. Guo, W. Hu, W. Hong, and W. Xie, Phys. Rev. A **99**, 043816 (2019).
26 A. Lukashchuk, J. Riemensberger, A. Tusnin, J. Liu, and T. J. Kippenberg, Nat. Photon. **17**, 814 (2023).
27 R. Chen, H. Shu, B. Shen, L. Chang, W. Xie, W. Liao, Z. Tao, J. E. Bowers, and X. Wang, Nat. Photon. **17**, 306 (2023).
28 A. R. Bishop, and P. S. Lomdahl, Phys. D **18**, 54 (1986).
29 L. A. Lugiato, and R. Lefever, Phys. Rev. Lett. **58**, 2209 (1987).
30 K. Nozaki, and N. Bekki, Phys. Rev. Lett. **50**, 1226 (1983).
31 K. J. Blow, and N. J. Doran, Phys. Rev. Lett. **52**, 526 (1984).
32 E. Shlizerman, and V. Rom-Kedar, Phys. Rev. Lett. **96**, 024104 (2006).
33 J. Xu, T. Zhao, P. Chang, C. Wang, and A. Wang, Opt. Lett. **48**, 3653 (2023).
34 D. Moreno, S. Fujii, A. Nakashima, D. Lemcke, A. Uchida, P. Sanchis, and T. Tanabe, Opt. Express **32**, 2460 (2024).
35 K. Myneni, T. A. Barr, B. R. Reed, S. D. Pethel, and N. J. Corron, Appl. Phys. Lett. **78**, 1496 (2001).
36 F. Y. Lin, and J. M. Liu, IEEE J. Quantum Electron. **40**, 815 (2004).
37 G. D. VanWiggeren, and R. Roy, Science **279**, 1198 (1998).
38 A. Argyris, D. Syvridis, L. Larger, V. Annovazzi-Lodi, P. Colet, I. Fischer, J. García-Ojalvo, C. R. Mirasso, L. Pesquera, and K. A. Shore, Nature **438**, 343 (2005).
39 L. Larger, and J. M. Dudley, Nature **465**, 41 (2010).
40 A. Uchida, K. Amano, M. Inoue, K. Hirano, S. Naito, H. Someya, I. Oowada, T. Kurashige, M. Shiki, S. Yoshimori, et al., Nat. Photon. **2**, 728 (2008).
41 I. Reidler, Y. Aviad, M. Rosenbluh, and I. Kanter, Phys. Rev. Lett. **103**, 024102 (2009).
42 I. Kanter, Y. Aviad, I. Reidler, E. Cohen, and M. Rosenbluh, Nat. Photon. **4**, 58 (2010).
43 K. Hirano, T. Yamazaki, S. Morikatsu, H. Okumura, H. Aida, A. Uchida, S. Yoshimori, K. Yoshimura, T. Harayama, and P. Davis, Opt. Express **18**, 5512 (2010).
44 L. Zhao, W. Xie, M. Wu, Y. Xiao, Z. Shen, J. Deng, H. Li, Z. Wu, J. Yang, W. Wei, et al., Laser Photonics Rev. e00671 (2025).
45 K. E. Chlouverakis, and M. J. Adams, Electron. Lett. **41**, 359 (2005).
46 J. Kim, J. Kang, T. Kim, and S. Han, Electronics Letters **42**, 1 (2006).
47 C. Godey, I. V. Balakireva, A. Coillet, and Y. K. Chembo, Phys. Rev. A **89**, 063814 (2014).
48 L. Fan, J. Wang, L. T. Varghese, H. Shen, B. Niu, Y. Xuan, A. M. Weiner, and M. Qi, Science **335**, 447 (2012).
49 L. Yuan, S. Xu, and S. Fan, Opt. Lett. **40**, 5140 (2015).
50 D. Pinto-Ramos, K. Alfaro-Bittner, M. G. Clerc, and R. G. Rojas, Phys. Rev. Lett. **126**, 194102 (2021).
51 L. Li, C. Hou, G. Wu, Y. Ruan, S. Chen, L. Yuan, and Z. Ni, Phys. Rev. B **110**, L041103 (2024).
52 L. Bakemeier, A. Alvermann, and H. Fehske, Phys. Rev. Lett. **114**, 013601 (2015).
53 S. E. Harris, and A. V. Sokolov, Phys. Rev. Lett. **81**, 2894 (1998).
54 F. L. Kien, J. Q. Liang, M. Katsuragawa, K. Ohtsuki, K. Hakuta, and A. V. Sokolov, Phys. Rev. A **60**, 1562 (1999).
55 F. L. Kien, K. Hakuta, and A. V. Sokolov, Phys. Rev. A **66**, 023813 (2002).
56 M. Zhi, X. Wang, and A. V. Sokolov, Opt. Express **16**, 12139 (2008).
57 K. Nozaki, and N. Bekki, Phys. D **21**, 381 (1986).
58 A. K. Tusnin, A. M. Tikan, and T. J. Kippenberg, Phys. Rev. A **102**, 023518 (2020).
59 Q. Shan, D. Yu, G. Li, L. Yuan, and X. Chen, PIER **169**, 33 (2020).
60 R. Boyd, Nonlinear Optics 3rd Edition. Burlington: Academic Press (2008).
61 M. Zhi, and A. V. Sokolov, Opt. Lett. **32**, 2251 (2007).
62 D. J. Little, M. Ams, P. Dekker, G. D. Marshall, J. M. Dawes, and M. J. Withford, Opt. Express **16**, 20029 (2008).
63 D. J. Wilson, K. Schneider, S. Hönl, M. Anderson, Y. Baumgartner, L. Czornomaz, T. J. Kippenberg, and P. Seidler, Nat. Photon. **14**, 57 (2020).
64 S. Lee and K. Krischer, Chaos. **31**, 113101 (2021).
65 K. Höhlein, F. P. Kemeth, and K. Krischer, Phys. Rev. E **100**, 022217 (2019).
66 M. Dinu, F. Quochi, and H. Garcia, Appl. Phys. Lett. **82**, 2954 (2003).
67 C. K. Sun, S. W. Chu, S. Keller, and S. P. DenBaars, Conference Digest. 2000 International Quantum Electronics Conference (Cat. No. 00TH8504), (IEEE2000).
68 J. H. Parker, D. W. Feldman, and M. Ashkin, Phys. Rev. **155**, 712 (1967).
69 W. M. Haynes, CRC Handbook of Chemistry and Physics. Boca Raton: CRC press (2016).
70 D. Yu, W. Song, L. Wang, R. Srikanth, S. Kaushik Sridhar, T. Chen, C. Huang, G. Li, X. Qiao, X. Wu, et al., Photon. Insights **4**, R06 (2025).
71 D. Leykam, and Y. D. Chong, Phys. Rev. Lett. **117**, 143901 (2016).
72 D. Zou, R. Liu, Y. Shi, A. Zhang, J. Li, G. J. Chen, H. Dang, Y. Song, M. Hu, and P. P. Shum, Adv. Photonics **7**, 016005 (2025).
73 A. Mucci, P. Suret, F. Copie, S. Randoux, R. Mullyadzhanov, and A. Gelash, Phys. Rev. Lett. **134**, 193804 (2025).
74 N. Englebert, N. Goldman, M. Erkintalo, N. Mostaan, S. P. Gorza, F. Leo, and J. Fatome, Nat. Phys.. **19**, 1014 (2023).
75 O. E. Örsel, J. Noh, P. Zhu, J. Yim, T. L. Hughes, R. Thomale, and G. Bahl, Phys. Rev. Lett. **134**, 153801 (2025).
76 M. Moenster, G. Steinmeyer, R. Iliew, F. Lederer, and K. Petermann, Opt. Lett. **31**, 3249 (2006).
77 P. Li, Y. C. Wang, and J. Z. Zhang, Opt. Express **18**, 20360 (2010).